

# Automated Discovery of Interactions and Dynamics for Large Networked Dynamical Systems

Yan Zhang<sup>1</sup>, Yu Guo<sup>2,3</sup>, Zhang Zhang<sup>1</sup>, Mengyuan Chen<sup>1</sup>, Shuo Wang<sup>1</sup>, and Jiang Zhang<sup>1,\*</sup> 

<sup>1</sup>Beijing Normal University, Beijing, China

<sup>2</sup>State Key Laboratory for Novel Software Technology at Nanjing University, Nanjing, China

<sup>3</sup>Software Institute, Nanjing University, Nanjing, China

\*zhangjiang@bnu.edu.cn

## ABSTRACT

Understanding the mechanisms of complex systems is very important. According to specific dynamic rules, a networked dynamical system, understanding a system as a group of nodes interacting on a given network, is a powerful tool for modelling complex systems. However, finding such models according to time series of behaviours is difficult. Conventional methods can work well only on small networks and for some types of dynamics. This paper proposes a unified framework for an automated interaction network and dynamics discovery (AIDD) on various network structures and dynamics, based on a stochastic gradient descent algorithm. The experiments show that AIDD can be applied to large systems with thousands of nodes and is robust against noise and missing information. We further propose a new method to test data-driven models based on control experiments. The results show that AIDD is able to learn the real network dynamics correctly.

## Introduction

Living cells, brains, human society, stock markets, global climate systems, and so forth are complex systems composed of many nonlinear interactive units [1–5]. By decomposing a complex system into a static network with dynamics on nodes, networked dynamical system models are powerful tools to describe complex systems, playing a paramount role in understanding their collective behaviours and controlling their functions [2, 3, 6]. However, building such models requires professional knowledge and modelling experience, which hinders the wide application of these methods. The reconstruction of such networked dynamical systems in a data-driven way remains a fundamental problem, i.e., to retrieve the interaction network structure and the node dynamics from time-series data of complex system behaviours without any subjective biases [7, 8].

Although many classical approaches to time series forecasting have been proposed [9, 10], prediction of the behaviours of complex systems with highly nonlinear and long-range correlations, especially those based on a complex network structure, had not been resolved until the recent introduction of graph (neural) network (GNN) models [11–22]. GNNs are designed particularly for networked dynamical systems. By learning complex functions of information aggregation and propagation on a given network, GNNs can simulate any complex dynamics on such networks. However, a complete graph is always required for most GNN models, which hinders their wider applications [8, 19, 23–26].

How to reveal network structure from time series data is of great importance because the revealed interaction network can not only help us to understand the behaviours of complex systems but also can improve algorithms' explainability and transparency in terms of causality [5, 27–30]. The interdependence relations or causal structure can be obtained by directly calculating some statistical measures [31–33], perturbing the system [34, 35], optimising a score function [36, 37], or expanding the complex interaction dynamics on a set of basal functions [7, 38, 39], and other methods [40–42].

Among these algorithms, the algorithm for revealing network interactions (ARNI) [43] is one of the most prominent methods. It can not only infer a network with high accuracy but can also be adopted for various nonlinear dynamics. However, one disadvantage is that the performance of the model strongly depends on the choice of the basal functions. If the prior biases on basal functions are missing, this approach becomes very time-consuming, limiting its application to larger systems.

Very few studies have been proposed to perform both network inference and time series forecasting tasks together, although some network inference algorithms are capable of forecasting. The implicit and time-variant network structures can also be obtained from deep learning models for forecasting based on an attention mechanism [8, 25, 44–47]. The first framework to derive an explicit network is NRI (neural relation inference) [19], in which an encoder–decoder framework is used. However, the complicated encoding process to infer the connections from time series data has limited scalability and accuracy on larger

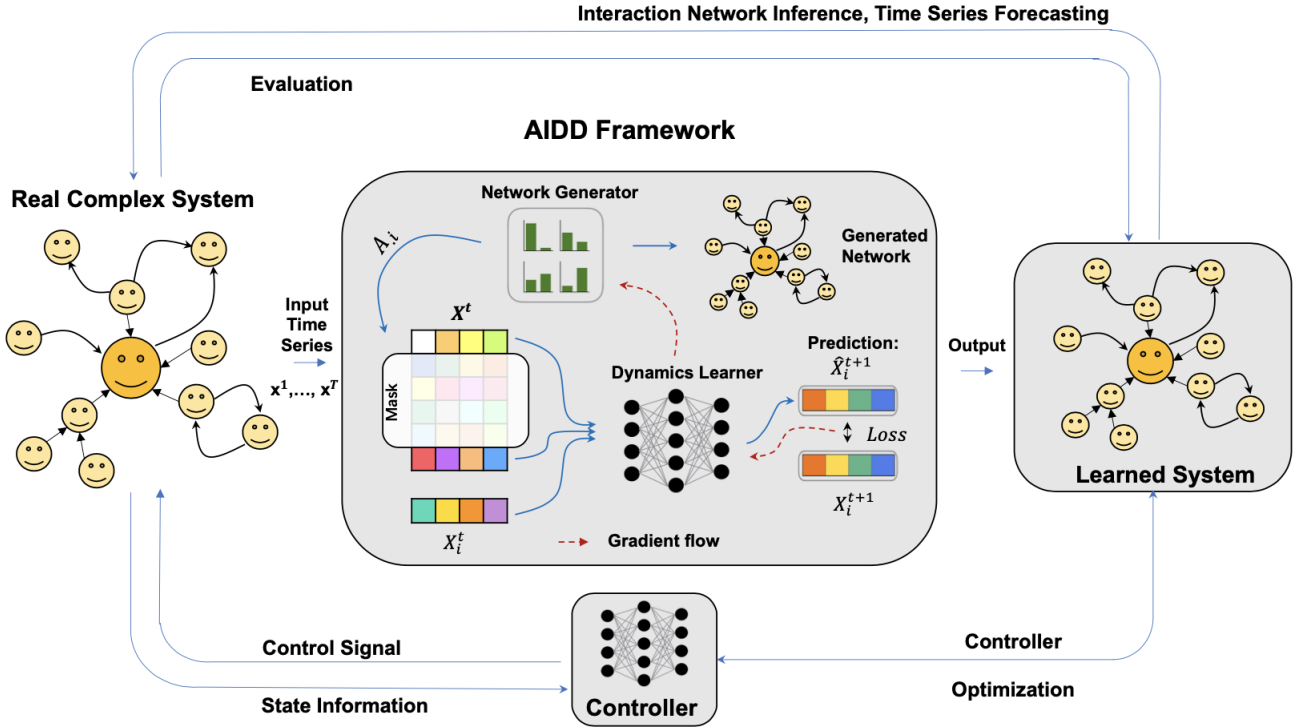


**Figure 1.** The workflow and evaluation of Automated Interaction and Dynamics Discovery (AIDD). Workflows showing how our proposed AIDD framework models a complex system, and how can be evaluated on tasks of time series forecasting, interaction network inference, and control experiments. The framework of the AIDD is also shown in the inset box. A column of the adjacency matrix for the candidate network is sampled by the network generator. It can be regarded as a mask vector to filter out the supposed unrelated nodes. Then, the time series information for related nodes is input into the dynamics learning module, which then outputs a prediction for the new states of all nodes. After that, the prediction is compared against the data. The loss function can be calculated, and the gradient information can be back-propagated directly. After optimisation, a learned networked dynamical system represented by neural networks can be obtained.

networks [24]. Further studies promote NRI on several aspects, such as the consideration of constraints [23, 48], and inferring hidden nodes [49], whereas the problem of scalability and accuracy remains.

However, despite the large number of experiments on evaluating and comparing various data-driven models that have been conducted based on prediction tasks, much room for improvement remains. According to the three-layer causal hierarchy, intervention and counterfactual experiments rather than predictions are the gold standards for testing a trained data-driven model as a complete substitution of the original system [27, 50]. That is, downstream tasks such as the control experiments of both the learned model and the original systems should be tested and compared [51]. However, we found only a few studies have performed this kind of task [6, 51].

As shown in Fig. 1, this paper proposes a unified framework for automated interactions and dynamics discovery (AIDD). This is a universal framework for learning both the interaction structure and dynamics of a complex system from time series data. The design of a lightweight network generator and a universal dynamics learning component based on Markov dynamics makes AIDD not only applicable to various networks and dynamics, but also enables it to reconstruct very large networks with high accuracy and robustness. The entire framework is differentiable so that it can be optimised directly by automatic differentiation and machine learning techniques [52]. Beyond tasks of network inference and time series forecasting, we propose a new method to test a learned data-driven model based on control experiments. Finally, we test the validity of our framework on real gene regulatory networks under noisy, incomplete, and interrupted data, which is close to realistic situations. The results demonstrate that a high performance can be obtained.

## Results

### Problem Formulation

Suppose the complex system to be considered evolves under discrete time steps. Thus, the dynamics to be reconstructed can be described by a mapping.

$$\mathbf{X}^{t+1} = f(\mathbf{X}^t, A) + \zeta^t, \quad (1)$$

where  $\mathbf{X}^t = [X_1^t, X_2^t, \dots, X_N^t] \in \mathbb{R}^{N \times D}$  is the state of the system at time  $t$ ,  $N$  is the number of nodes,  $D$  is the dimension of the state space of each single node,  $A$  is the adjacency matrix of the interaction network to be inferred, and  $\zeta^t \in \mathbb{R}^{N \times D}$  is the noise imposed on nodes. However, Equation 1 can only describe the dynamical processes with explicit mathematical forms and cannot be applied to those defined by rule tables or transitional probabilities, such as cellular automata, Boolean dynamics, or Markov chains. Therefore, instead of Equation 1, we use a more general form, a Markov chain  $\{\mathbf{X}^t\}$ , to describe the dynamics.

$$f(\mathbf{X}^{t+1} | \mathbf{X}^t, A) \equiv P(\mathbf{X}^{t+1} | \mathbf{X}^t, A), \quad (2)$$

where  $f$  is the dynamics to be discovered,  $\mathbf{X}^t$  is the abbreviation for the event that the random variable  $\mathbf{x}^t$  takes value  $\mathbf{x}^t \in S^N$ , where  $S$  is the state space of each single node and can be either a finite set of discrete values or an infinite set with continuous values.  $P$  is the conditional probability. Equation 2 is compatible with Equation 1 but more general [53]. It can even be extended to non-Markov random processes with finite histories by adding more hidden auxiliary variable variables[54].

However, it is difficult to infer the probabilities in Equation 2, particularly when  $N$  is large. Fortunately, the interactions of complex systems are always localised, which means that  $P(\mathbf{X}^{t+1} | \mathbf{X}^t, A)$  can be factorised into local transitional probabilities [55]:

$$P(\mathbf{X}^{t+1} | \mathbf{X}^t, A) = \prod_{i=1}^N P(X_i^{t+1} | \mathbf{X}^t \odot A_{.i}), \quad (3)$$

where  $\odot$  is the element-wise product, and  $A_{.i}$  represents the  $i^{\text{th}}$  column of matrix  $A$ , and  $\mathbf{X}^t \odot A_{.i}$  is a vector representing the state combination of all neighbour nodes of  $i$ . Then

$$f_i(X_i^{t+1} | \mathbf{X}^t \odot A_{.i}) \equiv P(X_i^{t+1} | \mathbf{X}^t \odot A_{.i}) \quad (4)$$

represents the local dynamics of node  $i$ , which is also called a causal mechanism in the literature [55].

Therefore, our task becomes the reconstruction of the network  $A$  and learning the local dynamics  $f_i$  according to the observed time series  $\mathbf{x} = (\mathbf{x}^1, \mathbf{x}^2, \dots, \mathbf{x}^T)$  with  $T$  time steps on multiple samples.

### Model

We build a neural network framework consisting of two modules to solve the reconstruction problem, as shown in the inset panel of Fig. 1. The first module is a network generator that can generate a candidate network adjacency matrix  $\hat{A}(\Theta)$  with the parameters  $\Theta$ . The second module then attempts to simulate the system dynamics  $f$  by using a set of neural networks  $\hat{f}_i(\hat{X}_i^{t+1} | \mathbf{x}^t \odot \hat{A}_{.i}(\theta_{.i}), \phi_i)$  for any node  $i$ , which are parameterized by  $\Phi = (\phi_1, \dots, \phi_N)$  to predict the future state  $\hat{\mathbf{X}}^{t+1}, \hat{\mathbf{X}}^{t+2}, \dots$  according to the candidate matrix  $\hat{A}(\Theta)$  and the observed state of the previous time step  $\mathbf{x}^t$ .

Instead of using the complicated graph network architecture to generate the candidate network as described in [19], we directly sample each element in the adjacency matrix  $\hat{A}_{ij} \sim \text{Bernoulli}(\theta_{ij})$ , where  $\theta_{ij} \in [0, 1]$  represents the probability that the entry of the  $i^{\text{th}}$  row and the  $j^{\text{th}}$  column in  $\hat{A}$  takes the value 1. To make the sampling process differentiable, we use the Gumbel-softmax technique [19, 56] to generate the adjacency matrix [24].

$$\hat{A}_{ij} = \sigma((\log(\theta_{ij}) + \xi_{ij}) / \tau), \quad (5)$$

where  $\xi_{ij} \sim \text{Gumbel}(0, 1)$  is a random number following the standard Gumbel distribution,  $\sigma$  is the softmax function, and  $\tau$  is the parameter of temperature to adjust the softness of the sampling process. The random numbers generated by Equation 5 have a similar distribution as  $\text{Bernoulli}(\theta_{ij})$ , especially when  $\tau$  is large. The simulated sampling process is differentiable such that the gradients can be passed by. When  $\tau \rightarrow \infty$ ,  $\hat{A}_{ij}$  exactly equals 1 with probability  $\theta_{ij}$ , or 0 with probability  $1 - \theta_{ij}$ .

Compared to other network generation mechanisms based on the Hadamard product of two  $V$  dimensional node feature vectors [8, 19, 44], where  $V \ll N$ , our method has higher accuracy in inferring links because more parameters ( $N \times N$  v.s.  $N \times V$ ) are used.

However, optimising  $N \times N$  parameters does not reduce the implementation performance because the matrix elements are independent of each other, which means that  $\hat{A}$  can be generated column-by-column separately, where each column represents the possible neighbourhood of a single node. In this way, our framework has a large improvement in flexibility and computational efficiency compared to the encoder-decoder frameworks such as [19] and can be applied to very large networks. However, the limitations are that the networks should be static, and the correlations between elements of  $\hat{A}$  are ignored. Further, the introduction of noise  $\xi_{ij}$  can push the network generator to jump out of local minimums during optimisation.

According to Equation 3, the dynamics learning module can also be decomposed into local modules node by node. Each local dynamics learner can be modelled by a feedforward or a recurrent neural network  $\hat{f}_i(\cdot|\phi_i)$ . Both the network structure and the parameters  $\phi_i$  can be shared by different nodes or not. If they share the dynamics learning module, they form a graph network [11, 19], as shown in Fig. 1.

## Objective function

Finally, the network inference and dynamics learning problem can be solved by minimising the following objective function.

$$\begin{aligned} L(\Theta, \Phi) &= \mathbb{E}_{\hat{A} \sim B(\Theta)} \left( - \sum_{t=1}^T \log P(\hat{\mathbf{X}}^{t+1} = \mathbf{x}^{t+1} | \mathbf{x}^t, \hat{A}, \Phi) \right) + \lambda \sum_{ij} \hat{A}_{ij} \\ &\approx - \frac{1}{K} \sum_{k=1}^K \sum_{t=1}^T \sum_{i=1}^N L_i(\hat{X}_i^{t+1} = x_i^{t+1} | \mathbf{x}^t, \hat{A}_{\cdot i}^k; \phi_i) + \lambda \sum_{ij} \hat{A}_{ij}, \end{aligned} \quad (6)$$

where

$$L_i(\hat{X}_i^{t+1} = x_i^{t+1} | \mathbf{x}^t, \hat{A}_{\cdot i}^k; \phi_i) = \log \hat{f}_i(\hat{X}_i^{t+1} = x_i^{t+1} | \mathbf{x}^t \odot \hat{A}_{\cdot i}^k; \phi_i) \quad (7)$$

is the local log-likelihood, and  $K$  is the number of samples for matrix  $\hat{A}$  under a given  $\Theta$ , and  $x_i^t$  is the observational vector of states of node  $i$  at time  $t$ . Thus, the objective function contains two terms, the former being the log-likelihood, which can be decomposed into local terms. The latter is the structural loss to conform the network to be sparse while avoiding over-fitting [48]. The parameter  $\lambda$  can adjust the relative importance of the structural loss. When we perform multiple time predictions, we can use  $\hat{\mathbf{X}}^t$  predicted by the previous time series instead of  $\mathbf{x}^t$  in Equation 7 to calculate the loss.

If the state space  $S$  of each node is real, then the local log-likelihood Equation 7 can be taken as a mean-absolute error (MAE) form,

$$L_i(\hat{X}_i^{t+1} = x_i^{t+1} | \mathbf{x}^t, \hat{A}_{\cdot i}^k) = \left| x_i^{t+1} - \hat{f}_i(\mathbf{x}^t \odot \hat{A}_{\cdot i}^k; \phi_i) \right|, \quad (8)$$

by assuming that  $\hat{f}_i(x_i^{t+1} | \mathbf{x}^t \odot \hat{A}_{\cdot i})$  is an independent Laplacian distribution for any data point  $\frac{1}{(2\nu)} \exp \left[ -\frac{1}{\nu} \cdot |x_i^{t+1} - \mu_i(\mathbf{x}^t \odot \hat{A}_{\cdot i} | \phi_i)| \right]$ , where, the mean value of the Laplacian distribution  $\mu_i$  is modelled by a neural network  $\hat{f}_i(\mathbf{x}^t \odot \hat{A}_{\cdot i}; \phi_i)$ , which can be regarded as a new form of the dynamics learner [57]. We let  $\nu = 1$  in this paper.

Then, the network dynamics to fit the observational data can be obtained by optimising the objective functions Equation 8 node by node [58]. We use the stochastic gradient descent algorithm to optimise. More details about training and testing can be found in the Methods section and the Supplementary Section 1.

## Performances and Comparisons

To test our model and compare it with others, we generate time series data by a set of network dynamics on a variety of graphs as the ground truths. All continuous, discrete, and binary dynamics are included. Spring (spring dynamics) [19], SIR (an inter-city meta-population SIR epidemic model) [59], and Michaelis–Menten kinetics [60, 61] all are examples of continuous dynamics. The coupled map network (CMN) [62, 63] and the voter model [64] are representatives of discrete and binary dynamics, respectively. The details of the dynamical models can be found in the Supplementary Section 6. The graphs to be inferred are either generated by models (ER [65] for Erdos Renyi, WS [4] for Watts-Strogatz, and BA [66] for Barabasi-Albert) or from empirical data including a gene network (for *S. cerevisiae*, Gene) [67], an inter-city traffic network (City) of China, three social networks (email, Dorm, and Blog), and a road network (Road) [68]. The details of the empirical networks can be found in the Supplementary Section 7. For each model and network, we ran the simulation for various lengths of time. All the reported results are on the testing dataset.

We compare our model to a series of baseline methods for both network inference and single step forecasting tasks. ARNI [43] and NRI [19] are both state-of-the-art models for network inference and time series forecasting. The former is based on the block-orthogonal regression method, and the latter is based on deep learning and graph networks. Two other

**Table 1.** Comparisons of performance on network inference and dynamics prediction tasks between AIDD and other selected methods (columns) on different dynamics and networks (rows)

Type	Model	Network	ARNI		MI	PC	NRI		LSTM	OURS	
			AUC	MSE	AUC	AUC	MSE/ACC	AUC	MSE/ACC	MSE/ACC	AUC
Con.	Spring	ER-10	0.5853	1.33E-03	0.7500	0.8250	<b>2.60E-08</b>	0.9998*	2.98E-04	2.70E-04*	<b>1.0</b>
		WS-10	0.5125	1.58E-03	0.6875	0.7875	<b>8.40E-08</b>	0.9997*	3.35E-04	3.31E-04*	<b>1.0</b>
		BA-10	0.5169	1.10E-03	0.6422	0.6571	<b>7.00E-10</b>	0.9999*	2.14E-04	2.90E-05*	<b>1.0</b>
		ER-2000	-	-	0.4997	-	-	-	2.25E-03	<b>1.18E-05</b>	<b>0.9886</b>
		WS-2000	-	-	0.5002	-	-	-	5.89E-03	<b>8.51E-06</b>	<b>0.9933</b>
	BA-2000	-	-	0.5010	-	-	-	4.54E-03	<b>2.09E-03</b>	<b>0.9523</b>	
	SIR	SIR-371(D)	0.5424*	8.25E-03	0.5027	0.5119	-	-	2.28E-03*	<b>2.98E-05</b>	<b>0.9156</b>
Menten	Gene-100(D)	<b>1.0</b>	9.71E-03	0.5416	0.6574	-	-	2.29E-03*	<b>4.37E-05</b>	0.9960*	
Dis.	CMN	ER-10	<b>1.0</b>	<b>2.33E-09</b>	0.5745	0.7804	1.40E-05	0.8850	2.60E-04	5.60E-06*	<b>1.0</b>
		WS-10	<b>1.0</b>	<b>2.35E-09</b>	0.6875	0.8375	9.40E-06	0.9331	2.40E-04	2.80E-06*	<b>1.0</b>
		BA-10	<b>1.0</b>	<b>2.40E-09</b>	0.4390	0.7439	1.30E-05	0.6753	9.21E-05	6.90E-06*	<b>1.0</b>
		ER-200	0.8441*	4.17E-02	0.5774	0.7648	-	-	5.91E-05	<b>2.04E-06</b>	<b>0.9987</b>
		WS-200	<b>1.0</b>	<b>2.36E-09</b>	0.6969	0.7506	-	-	1.63E-04	1.95E-06	0.9987*
		BA-200	0.8840*	2.45E-02	0.5533	0.7493	-	-	1.46E-04	<b>2.57E-06</b>	<b>0.9874</b>
		WS-1000	-	-	0.5670	-	-	-	3.54E-05	<b>2.92E-06</b>	<b>0.9795</b>
		BA-1000	-	-	0.5290	-	-	-	<b>3.46E-05</b>	5.48E-05	<b>0.9105</b>
		Bin.	Voter	ER-10	-	-	-	0.4552	0.8447*	0.5000	0.5242
WS-10	-			-	-	0.5250	0.9062*	0.5037	0.6007	<b>0.9463</b>	<b>1.0</b>
BA-10	-			-	-	0.4607	0.9588*	0.4999	0.6917	<b>0.9866</b>	<b>1.0</b>
WS-1000	-			-	0.5470*	-	-	-	0.5317	<b>0.6650</b>	<b>0.9996</b>
BA-1000	-			-	0.5030	-	-	-	0.5208*	<b>0.6758</b>	<b>0.9942</b>
EMAIL-1133	-			-	0.4999	-	-	-	0.5333*	<b>0.7212</b>	<b>0.9576</b>
ROAD-1174	-			-	0.5004	-	-	-	0.5455*	<b>0.8942</b>	<b>0.9996</b>
DORM-217(D)	-			-	0.5219	-	-	-	0.5735*	<b>0.6951</b>	<b>0.9901</b>
BLOG-1224(D)	-			-	0.4995	-	-	-	0.5295*	<b>0.6793</b>	<b>0.8603</b>

In the network column, we use network - size format. The networks marked with “D” means that they are directed graphs. All networks generated by models share the same edge density value, which is 1% for large networks (size > 10), and it is 20% and 3% for small networks with sizes smaller than 10, and ER networks with size = 200, respectively, to avoid isolated nodes. All the results are the averages of five repeated experiments. The same data volume is shared for different methods in one row. The items marked by “-” indicate that valid results of the model cannot be obtained due to the limitations of the specific method on dynamics, memory, or time consumption. The best results among all the compared algorithms in the same row are boldfaced, and the second-best results are marked “\*”. More parameter settings are shown in the Supplementary Section 9.

frequently used statistical metrics, partial correlation and mutual information, are also compared on the network inference task. In addition, the classic time series forecasting model, long short-term memory (LSTM) [54], is compared on the prediction task. The details of these comparison models can be found in the Supplementary Section 5. In all the experiments, we used a graph network with 128 hidden units as the dynamics learning module (see the method section for details). The neural network is shared by all nodes. Other parameters are shown in the footnote of Table 1 and Supplementary Section 9.

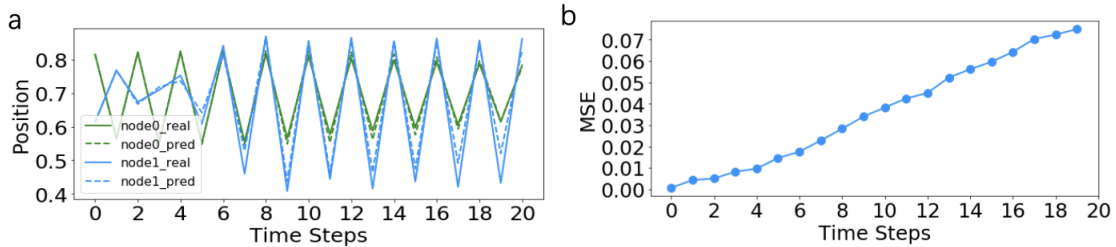


**Figure 2.** Multi-step prediction results of AIDD on CMN dynamics data in a 10-node ER network. In (a), we show the time series data of multi-step predictions and the ground truths for two selected nodes. In (b), we show how the mean square error (MSE) increases with time for CMN dynamics. The parameters are the same as in Table 1.

As shown in Table 1, our model outperforms all the methods on large networks for both tasks. Compared with the ARNI model, AIDD does not rely on the choice of basis functions; as a result, it can be applied to very diverse dynamics. By using neural networks as a universal estimator for dynamics, AIDD avoids the problem of combinatorial explosion of basis functions. This enables AIDD to have competitive performances on space and time complexity ( $O(N^2)$  v.s.  $O(N^3)$  for ARNI. In ARNI model, the time complexity of finding the interactions of a single node is  $O(N^2)$ , so the time complexity of revealing the entire

network interactions is  $O(N^3)$ ). In order to compare performance on time series forecasting, we slightly modified the original algorithm of ARNI such that it can also output one-step prediction [43]. Compared to the NRI framework, our model has a much lighter network generation architecture. NRI cannot output any result under the same limitations of time and space on networks with sizes larger than 30 owing to the computational complexity [19].

The model can also output multi-step prediction results by feeding the result of the one-step prediction output back to the model. Figure 2 shows the results for the selected dynamics.

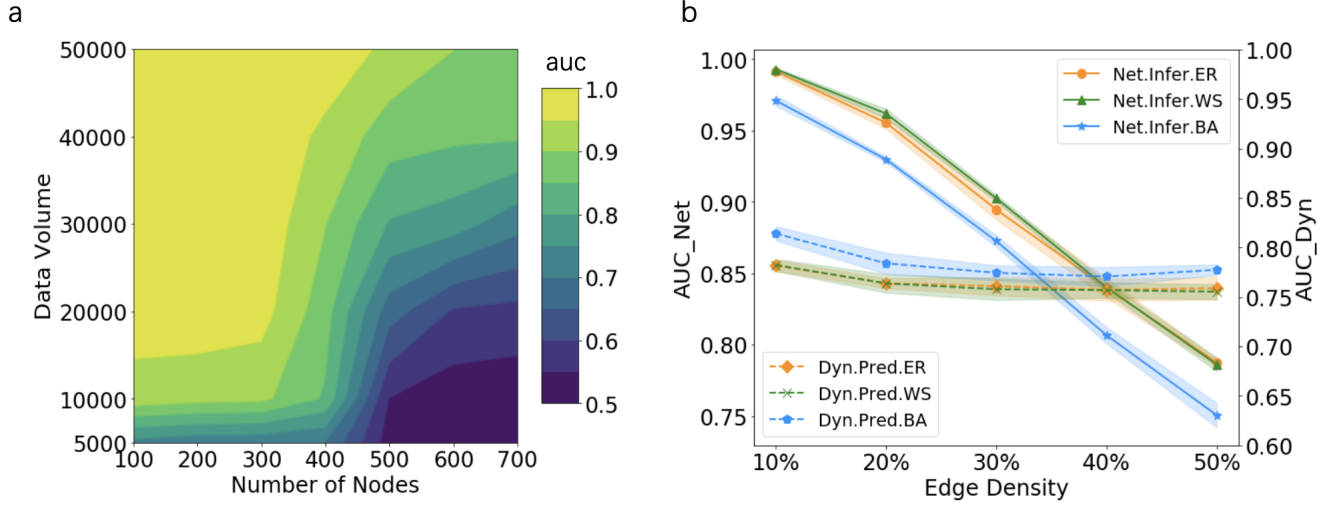


**Figure 3.** The performance of AIDD under different factors in network inference and dynamics learning. (a) shows how the number of nodes and the volume of data (the number of samples  $\times$  the number of time steps, which was fixed to 100) jointly influence the network inference accuracy on WS networks under CMN dynamics. With the exception of 100 nodes with a 4% edge density, all nodes shared the same edge density value, which was 1%. (b) shows how performance decreases with edge density. For the experiments in (b), we set the number of nodes to 100, and the sparse matrix parameter  $\lambda$  was set to 0.

In general, AIDD works very well on large sparse networks, and the performance on both tasks decreases as the edge density increases, as shown in Fig. 3(b).

We can improve the accuracy by increasing the amount of data. Figure 3(a) shows how the area under curve (AUC) depends on both network size and data volume to be fed into the model systematically, and similar contours can be obtained on MSE errors (see Supplementary Section 2). There is a trade-off between network size and data volume under a given accuracy, as shown in Fig. 3(a). It is interesting to observe that data volume is sensitive to network size only when the number of nodes is between 300 and 500, and beyond that, a minimum amount of data volume is sufficient to obtain an acceptable accuracy (e.g.,  $AUC = 0.7$ ), and this almost does not depend on how large the network is. We suppose that the given total number of epochs is sufficient for training the model only for networks smaller than 300, which is the reason why a sudden increase in data volume is observed. When the size is larger than 500, the model can converge quickly when sufficient data volume is provided; therefore, the curves become insensitive again.

### Robustness against noise and hidden nodes

A good data-driven model must be robust against noise and unobservable nodes such that it can be applied to the real world. To show the robustness against noise of AIDD, we plot changes in AUC with the magnitude of noise on Michaelis–Menten kinetics [60, 61], which can describe the dynamics of Gene regulatory networks, as shown in Fig. 4. Our model can recover the network structure with 0.85 AUC when the mean magnitude of noise is 0.3.

In real applications, we can only obtain partial information of the entire system owing to the limitations of observation. Thus, a certain proportion of nodes are unobservable or hidden. This requires the inference algorithm to be robust to hidden nodes. Thus, we test the AIDD on an incomplete network. To generate the incomplete network data as the ground truth, we randomly select a certain percentage of nodes as the hidden nodes (Fig. 4(a)), and the time series data of these nodes are removed. AUC decreases and MSE increases as the fraction of the number of unobserved nodes increases on both spring and voice dynamics, as shown in Fig. 4(c); however, the sensitivity depends on various types of dynamics. It is found that when the proportion of missing nodes reaches 50%, the inference accuracy is still above 95%, which proves that our model can achieve superior results in the absence of normally sufficient amounts of data.

Furthermore, we test the ability of AIDD to reveal unknown network structures of unobservable nodes on CMN and Voter dynamics, with only the number of hidden nodes available. We completed this task by performing the same interaction inference task, setting the states for unknown nodes to random values. Figure 4(d) shows the AUCs of the link structures of unknown networks on Voter and CMN dynamics. The results reveal that the network inference accuracy is robust for missing nodes. The algorithm can recover the interactions even for unobservable nodes with over 80% accuracy. The details of the algorithm can be found in [69] and Supplementary Section 3.

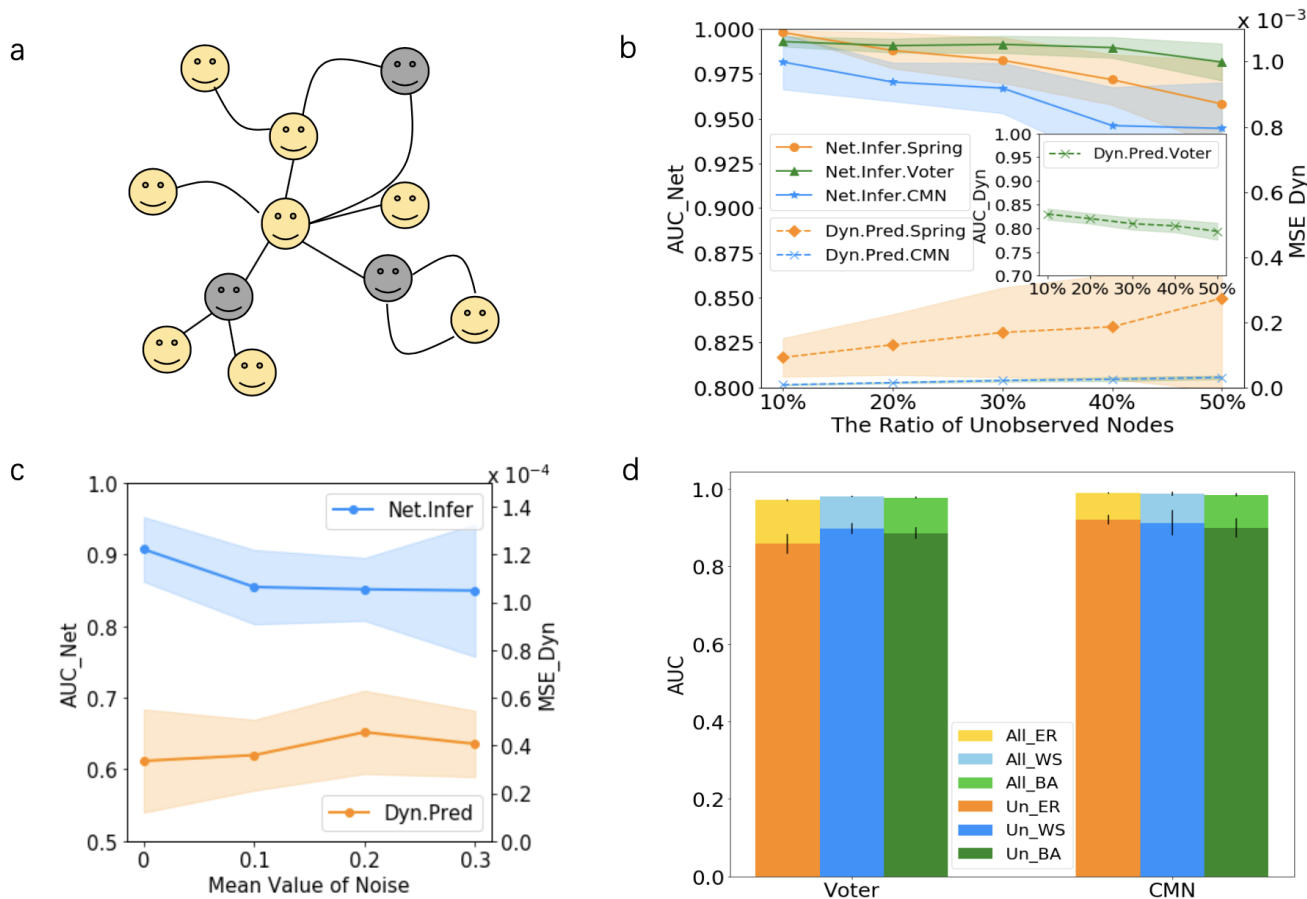


**Figure 4.** The robustness evaluation of AIDD against noise and missing nodes. (a) shows a schematic ground truth network with missing information on the unobserved nodes (grey nodes). (b) shows the influence of proportion of unobserved nodes on the accuracy of interaction inference on the partial network with observed nodes measured by AUC, and the accuracy of dynamic predictions (inset) measured by the MSE of the observable nodes on Spring, CMN, and the AUC of the observable nodes on Voter dynamics. All the experiments were conducted on an ER network with 100 nodes, and all networks generated by models share the same edge density value, which is 4%. (c) shows the dependence of AUC and MSE on the mean of noise added on each node for the Michaelis–Menten kinetics (Gene dynamics) on the yeast *S. cerevisiae* gene network with 100 nodes. (d) shows the ability of AIDD to infer interactions on the entire network (the light colour bars) and the unobserved partial networks (the dark colour bars). All the experiments are conducted on CMN and Voter dynamics with ER, WS, and BA networks, and all networks contain 100 nodes with 10% unobservable nodes selected randomly, and all networks generated by models share the same edge density value, which is 4%. The parameters in these experiments can be referred to in the Supplementary Section 9.

## Control

To further verify that AIDD has learned the ground truth dynamics and that the trained model can replace the original system, we design control experiments. The reasons why we choose the control problem as the test bed for our model include (1) the control problem in a complex network is very important, and it has relevance to many engineering fields [6]; (2) the control problem is more difficult than predictions. This is true because to control a system means to intervene in it. As a result,

we have stood at least on the second level of the causal hierarchy [50].

Here, our control problem is to find a control law based on the learned network dynamics such that if the rule is applied to the ground truth model, we can synchronise the whole system by regulating a few nodes. To do this, we divide the nodes in the network into two groups: the driver nodes, who can be manipulated by the controller directly, and the target nodes, whose states cannot be directly controlled, but can be influenced indirectly. The controller is designed by optimising a set of parameters such that the control objective, that is, the synchronisation of the whole system, is achieved.

The control experiments consisted of two stages as shown in the bottom part of Fig. 1. In the first stage, we find the optimised controller's parameters on the learned network dynamics to achieve the designed objective. In the second stage, we apply the optimised controller to the ground truth model. In order to verify the learned model, we also optimize another controller on the ground truth model. After that, we compare the deviation curves of the two controllers from the control target on the same ground truth model. If the curves are similar, we conclude that the learned model can substitute for the real model. The detailed methods can be referred to in the Supplementary Section 4.

Two control experiments were designed. The first problem is to synchronise the movement directions of all masses with spring dynamics on a small-size BA network with 10 nodes (see Fig. 5(a)). Three nodes with the largest degrees are selected as the driver nodes. The controller implemented by a neural network adjusts the forces imposed on the drivers according to the current state of the system at each time step. The experimental results are shown in Fig. 5. The two MSE curves in Fig. 5(b) depict the degree of control achieved by the trained model and the ground truth model, respectively. They overlap to show that the learned dynamics can be a good substitute for the real system. Both curves approached 0 within 13 timesteps, indicating that the controllers achieved the goal within the given time.

The second control experiment involves querying all the oscillators in a CMN model on a WS model network with 10 nodes (see Fig. 5(d)) to take the same value of 0.6, which is the mean value an oscillator can take with a given range. The controller is a parameterized neural network, which maps the current state of the system into the control signals (see Supplementary Section 4). The signals are the forces imposed on the two drivers (with the largest degrees) directly. From Fig. 6 (e) and (f), the controls are not well achieved for all nodes because the MSE curves do not converge to zeros. However, the two MSE curves overlap very well, indicating that the surrogate behaves identically to the ground truth model.

## Gene regulatory network inference

To verify that our algorithm can be applied to actual scenarios and not only on toy models, we attempt to infer the real subnetwork structure from the known transcriptional network of yeast *S. cerevisiae* according to the time series data of mRNA concentrations generated by GeneNetWeaver (GNW) [67], a famous simulator for gene dynamics.

The networks used by GNWs are extracted from known biological interaction networks (*Escherichia coli*, *Saccharomyces cerevisiae*, etc.). On these networks, GNW uses a set of dynamical equations to simulate the transcription and translation processes, and it has considered many factors close to real situations (see Supplementary Section 6 for details). Therefore, GNW is a famous platform for benchmarking and performance assessment of network inference methods.

In the experiment, we used yeast *S. cerevisiae* gene network with 100 nodes as the benchmark gene network, and we used the default parameters of DREAM4\_In-Silico in GeneNetWeaver software to generate data. For the dynamics learner, we use different neural networks for each node because of the heterogeneity of node dynamics and the existence of latent variables, noise, and perturbations [67]. We compare our method with partial correlation, Bayesian network inference, and mutual information algorithms. Our method outperforms others on network inference (Fig. 6(a)) on the AUC(0.82). It can also predict the dynamics with a relatively high accuracy (the average absolute error (MAE) is 0.038, see Fig. 6. This indicates that our method can perform well realistic gene regulatory dynamics.

## Discussion

In this paper, we propose a unified framework of automatic interaction and dynamics discovery, called AIDD, for large network dynamical systems. We also propose a new standard based on control tasks to evaluate whether the true network dynamics can be learned.

The main highlights of AIDD include scalability, universality, and robustness. The high scalability is reflected by the fact that the model can be applied to large networks with more than thousands of nodes with more than 90% accuracy because the training procedure can be taken node by node. AIDD is a universal framework because it can be applied to various types of dynamics, including continuous, discrete, and binary. AIDD is robust not only on noisy input signals, but also on unobservable nodes. AIDD can recover an entire network even when time series data is missing with more than 90% accuracy. AIDD was also shown to work well on datasets generated by GeneNetWeaver, which emulates the real environment of gene regulatory network dynamics.

Furthermore, we propose a new method based on controls to test the validity of the learned model. We have optimised two controllers, one of which is optimised on the real system and the other is optimised on the model. Then, we apply them to

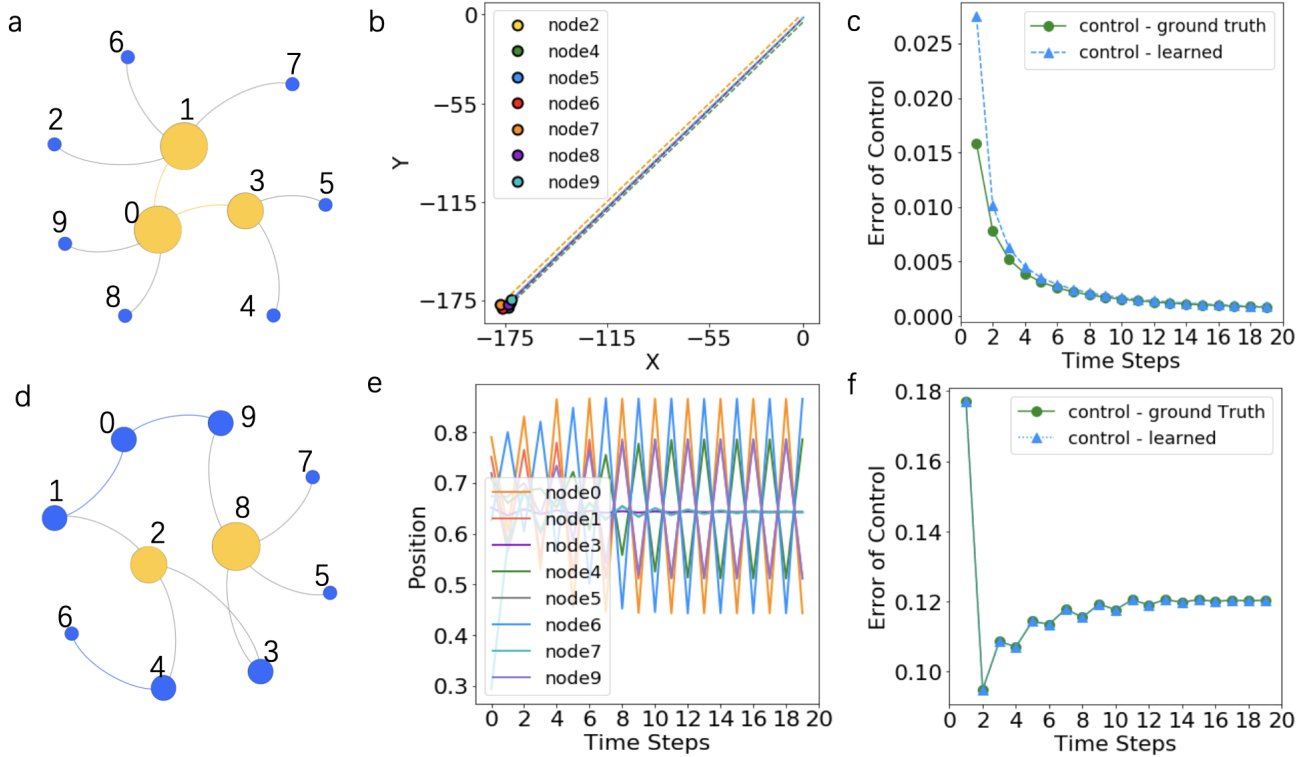


**Figure 5.** The control experiments on learned models. (a) shows the spring network that we studied for the first experiment. Three large nodes are driver nodes, and the others are target nodes. The control objective is to request all masses to have the same movement direction. (b) shows the final movement states of all the target nodes under the controls. (c) shows two MSE curves for evaluating goal achievement versus time steps of the controls. One represents the results of learned model, and the other is the ground truth. (d) is a coupled mapping network that we studied in the second experiment. Two large nodes were selected as driver nodes. The control objective is to ask all oscillators to have the same value of 0.6, which is the mean of the value range for all nodes. (e) shows the oscillations of all target nodes during control. (f) shows two MSE curves for evaluating goal achievement versus time steps of the controls. One is for the trained model, and the other for the ground truth. The parameters in these experiments are given in the Supplementary Section 9.

a real system. If they behave similarly, we conclude that the learned model can be a substitute for the real system. Control experiments on spring and CMN dynamics of small networks have proved that well-trained AIDD models can replace the real systems.

This framework has many potential applications. For example, AIDD can be used to infer missing links according to the dynamics information. AIDD can also be used in time series forecasting. In contrast to other forecasting models, a clear binary network can be output by AIDD, which can provide deeper insights into element interactions and potential causal links, increasing the explainability of the model.

However, some drawbacks are present in AIDD. First, a large amount of training data, especially the time series in diverse initial conditions, is required to obtain a good model. Nevertheless, it is difficult to obtain different time series under a variety of initial conditions. Although we can split a long time series into segments, and the first values on each segment can be treated as a new initial condition, the diversity of the initial conditions is always not high enough to train an AIDD model with high quality. Hence we may develop new models that are suitable for small data.

Second, all the dynamics considered in this paper are Markovian, but this property is hardly satisfied in real cases. New extensions and experiments on non-Markovian dynamics should be conducted. For example, we can use a recurrent neural network instead of a feed-forward network as the dynamics learning component.

Finally, our network generator samples networks according to the naive mean field assumption. Although good results have been obtained on network inference, correlations between nodes are ignored. Thus, we can use generative graph models to replace the Bernoulli network generator such that correlations and inductive bias on structures can be considered.

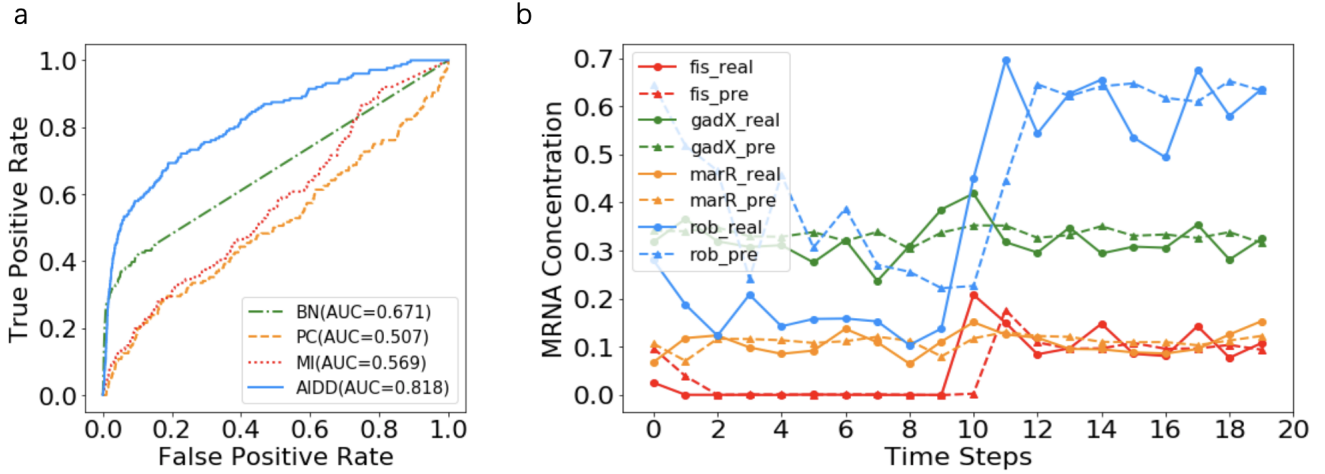


**Figure 6.** Performances of AIDD and other compared methods on network inference for the gene regulatory network of yeast *S. cerevisiae* with 100 nodes. (a) ROC curves of different network inference methods. The comparison methods include Bayesian network (BN), partial correlation (PC), mutual information (MI), and AIDD. The AUC for different methods is marked in the legend. (b) shows the comparison between the observed time series of the expression data (real) and the predicted data on selected genes. In this plot, the solid lines represent the predictions and the dotted lines represent the observed data.

## Methods

### AIDD

The framework consists of two parts: a network generator and a dynamics learner. The input of the model is the state information of all nodes at time  $t$ , and the output of the model is the predicted state information of all nodes at time  $t + 1$ . The inferred adjacency matrix  $\hat{A}$  can also be retrieved from the network generator.

The network generator is simply a differential matrix sampler parameterized by  $N^2$  parameters  $\Theta$ , as described in the model sub-section of the main text. However, the dynamics learners are different for different tasks. We will illustrate the details as follows.

#### Architecture of the Dynamics Learning module

In all experiments except the final one (the gene regulatory network inference from GeneNetWeaver generated data), we used the same neural network structure to construct the dynamics learning module, as shown in Fig. 7. The network structure and weights are shared by all nodes. This design has been verified to be suitable for learning various complex dynamics [19, 24].

In all experiments, we set the hidden layer size of the dynamics learner to 128. The parameter  $\tau$  in the network generator was set to 1. In the experiments, we set  $K$  to be the number of epochs because  $\hat{A}_i(\Theta)$  are sampled at each epoch.

The  $\lambda$  in the objective function is the coefficient of the sparse matrix. In the experiments where the number of nodes is less than 1000,  $\lambda$  is set to 0.0001, while  $\lambda$  is set to 0.001 for larger networks. More details about the parameters can be found in the Supplementary Section 9.

#### Architecture of AIDD for gene regulatory network inference

We adopt a heterogeneous network structure in the task of gene regulatory network inference because the regulation dynamics and parameters are heterogeneous for different genes. In detail, the dynamics learning module consists of several multi-layer perceptrons (MLPs), with each MLP corresponding to a single gene. The input of the MLP is a vector produced by the element-wise product of the gene expression vector  $\mathbf{X}^t$  and the column vector  $\hat{A}_i$  of the adjacency matrix, which represents the TF(transcription factors) regulation acting on the corresponding gene  $i$ . The output of the MLP is  $\hat{X}_i^{t+1}$ , which is the estimated concentration of gene  $i$  at time  $t + 1$ . The concatenation of all MLP outputs is the gene expression value  $\hat{\mathbf{X}}^{t+1}$  at time  $t + 1$ . Then, we can compare the output estimation  $\hat{\mathbf{X}}^{t+1}$  and the real expression value  $\mathbf{X}^{t+1}$  to compute the loss function. Then, the stochastic gradient descent algorithm can be applied to minimise the loss function. The structure diagram of the model is shown in Fig. 8.

### Training

We separate the training data by batches and use the stochastic gradient descent algorithm to update the parameters  $\Theta, \Phi$  step by step with different learning rates  $lr_\theta$  and  $lr_\phi$ , respectively, until the epochs of training exceed a threshold. The gradients

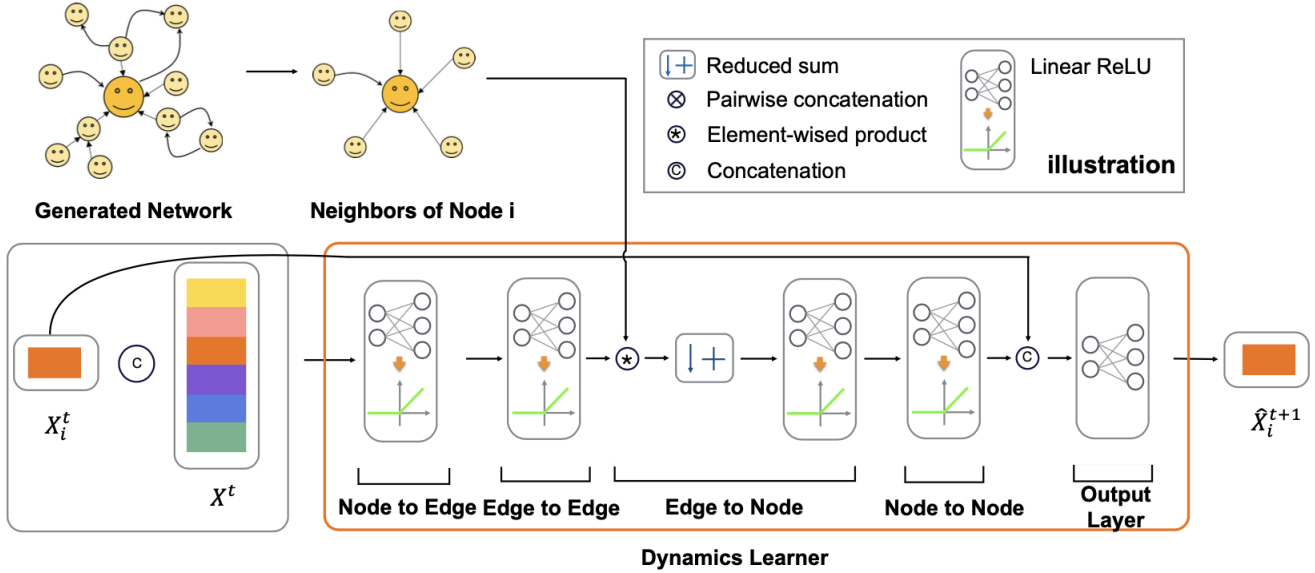


**Figure 7.** The feedforward process of the dynamics learning module. It can be divided into four steps. (1) Node to Edge: aggregating the original information of nodes to form representations of edges; (2) Edge to Edge: update the edge representations; (3) Edge to Node: aggregate all information on neighbouring edges of each node to form a new feature vector of the current node; (4) node to node: update the node representations; (5) Output: finally, concatenate the node representations and the input state vectors of node  $i$  to feed into a feedforward network, and output the prediction of the next state of  $i$ .

can be computed directly by the automatic differentiation technique on the Pytorch platform because all the steps in our framework are differentiable. To improve the efficiency, we sampled one adjacency matrix at each epoch and updated the parameters immediately. For the complete algorithm, readers are referred to the Supplementary Section 1. We implemented the gradient descent algorithm with the Adam optimizer, and all the algorithms were run on an RTX 2080Ti(11G).

### Network Inference and Time Series Forecasting

After sufficient training, the optimised parameters of  $\Theta^*$  and  $\Phi^*$  can be obtained. Then, we can use a network generator to sample the complete adjacency matrices as the inferred networks by setting  $\Theta = \Theta^*$  and  $\tau \rightarrow \infty$  to obtain absolute 0 or 1.

A single time-step prediction of states for all nodes can be sampled by using the dynamics learner  $\hat{\mathbf{x}}^{t+1} \sim P(\hat{\mathbf{X}}^{t+1} | \mathbf{x}^t, \hat{A}(\Theta^*), \Phi^*)$ , where  $\hat{A}(\Theta^*)$  is a sampled adjacency matrix by the optimal parameters. Multiple time-step predictions can also be obtained in an independent rollout manner [70], that is, sampling the state recursively,  $\hat{\mathbf{x}}^{t+1} \sim P(\hat{\mathbf{X}}^{t+1} | \hat{\mathbf{x}}^t, \hat{A}(\Theta^*), \Phi^*)$  for all  $t' > 0$ . Note that  $\hat{\mathbf{x}}^t$  represents the sample of  $\hat{\mathbf{X}}^t$  according to the dynamics learner.

Areas under the curve (AUC) and mean square errors (MSE for continuous values) or AUC (for binary values) are used to evaluate the results of network inference and time series forecasting, respectively. More details on training and evaluation can be found in the Supplementary Section 8 and 9.

### Data availability

We used the default parameters of DREAM4\_In-Silico in GeneNetWeaver software to generate gene network, GeneNetWeaver software can be download on <https://github.com/tschaffter/gnw> [67]. Three social networks (email, Dorm, and Blog), and a road network(Road) [68] can be found at [http://networkrepository.com/email-enron-only.php#collapse\\_ack](http://networkrepository.com/email-enron-only.php#collapse_ack).

### Code availability

AIDD code repository can be found at <https://github.com/kby24/AIDD>. The repository includes example codes for generating data and Algorithms of AIDD.

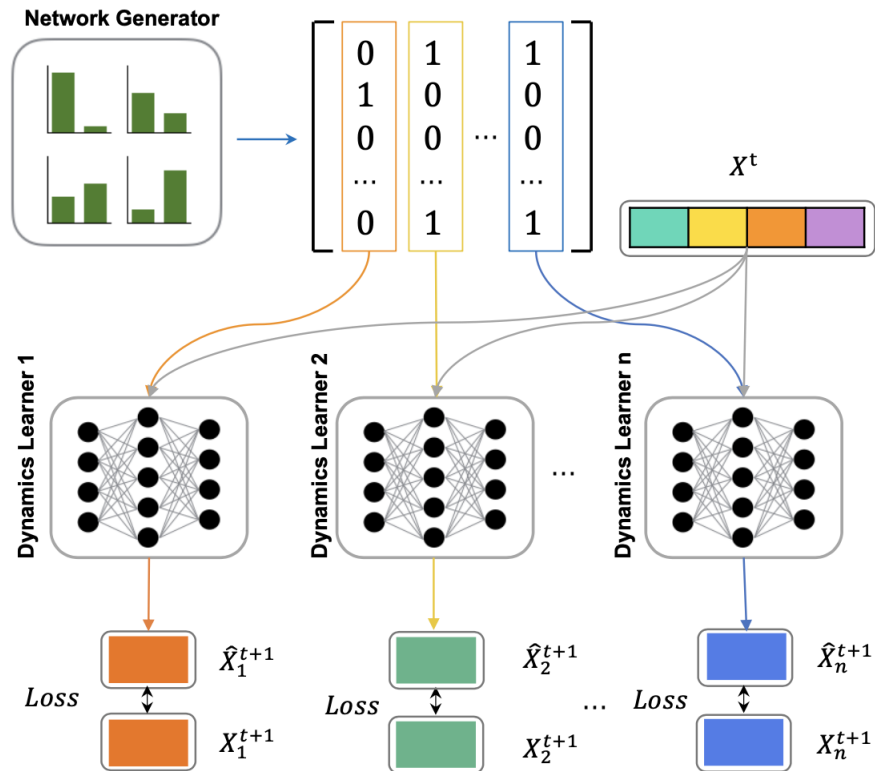


**Figure 8.** The architecture of AIDD in the task of gene regulatory network inference. The same network generator is used, but different dynamics learners are set for each node. In the forward process, the adjacency matrix is generated by the network generator through Gumbel softmax sampling. Then, the element-wise products between gene expression vector  $X^t$  at time  $t$  and column  $i$  of the adjacency matrix are calculated as the input for the corresponding dynamics learner  $i$ . Subsequently, the dynamics learner  $i$ , which is an MLP, computes the output  $\hat{X}_i^{t+1}$ , which is the estimation of gene  $i$ 's expression at time  $t + 1$ . The back-propagation process updates the network generator and dynamics learners simultaneously.

## References

1. Siegenfeld, A. F. & Bar-Yam, Y. An introduction to complex systems science and its applications. *Complexity* **2020** (2020).
2. Boccaletti, S., Latora, V., Moreno, Y., Chavez, M. & Hwang, D.-U. Complex networks: Structure and dynamics. *Phys.reports* **424**, 175–308 (2006).
3. Bullmore, E. & Sporns, O. Complex brain networks: graph theoretical analysis of structural and functional systems. *Nat.reviews neuroscience* **10**, 186–198 (2009).
4. Watts, D. J. & Strogatz, S. H. Collective dynamics of 'small world' networks. *Nature* **393**, 440–442 (1998).
5. Runge, J., Nowack, P., Kretschmer, M., Flaxman, S. & Sejdinovic, D. Detecting and quantifying causal associations in large nonlinear time series datasets. *Sci. Adv.* **5**, eaau4996 (2019).
6. Liu, Y.-Y. & Barabási, A.-L. Control principles of complex systems. *Rev. Mod. Phys.* **88**, 035006 (2016).
7. Wang, W.-X., Lai, Y.-C. & Grebogi, C. Data based identification and prediction of nonlinear and complex dynamical systems. *Phys. Reports* **644**, 1–76 (2016).
8. Ha, S. & Jeong, H. Deep learning reveals hidden interactions in complex systems. Preprint at <https://arxiv.org/abs/2001.02539> (2020).
9. Brockwell, P. J., Davis, R. A. & Fienberg, S. E. *Time Series: Theory and Methods* (Springer Science & Business Media, 1991).
10. Benidis, K. et al. Neural forecasting: Introduction and literature overview. Preprint at <https://arxiv.org/abs/2004.10240> (2020).
11. Scarselli, F., Gori, M., Tsoi, A. C., Hagenbuchner, M. & Monfardini, G. The graph neural network model. *IEEE Transactions on Neural Networks* **20**, 61–80 (2008).
12. Battaglia, P. W. et al. Relational inductive biases, deep learning, and graph networks. Preprint at <https://arxiv.org/abs/1806.01261> (2018).
13. Wu, Z. et al. A comprehensive survey on graph neural networks. *IEEE Transactions on Neural Networks Learn. Syst.* **32**, 4–24 (2021).
14. Zhou, J. et al. Graph neural networks: A review of methods and applications. Preprint at <https://arxiv.org/abs/1812.08434> (2018).
15. Zhang, Z., Cui, P. & Zhu, W. Deep learning on graphs: A survey. *IEEE Transactions on Knowl. Data Eng.* 1–1 (2020).
16. Yu, B., Yin, H. & Zhu, Z. Spatio-temporal graph convolutional networks: A deep learning framework for traffic forecasting. In *Proceedings of the Twenty-Seventh International Joint Conference on Artificial Intelligence IJCAI*, 3634–3640 (ijcai.org,2018).
17. Sanchez-Gonzalez, A. et al. Graph networks as learnable physics engines for inference and control. In *International Conference on Machine Learning*, 4470–4479 (PMLR, 2018).
18. Bapst, V. et al. Unveiling the predictive power of static structure in glassy systems. *Nat. Phys.* **16**, 448–454 (2020).
19. Kipf, T., Fetaya, E., Wang, K.-C., Welling, M. & Zemel, R. Neural relational inference for interacting systems. In *International Conference on Machine Learning*, 2688–2697 (PMLR, 2018).
20. Zhang, Z. et al. Neural gene network constructor: A neural based model for reconstructing gene regulatory network. Preprint at <https://www.biorxiv.org/content/10.1101/842369v1.abstract> (2019).
21. Zheng, C., Fan, X., Wang, C. & Qi, J. Gman: A graph multi-attention network for traffic prediction. In *Proceedings of the AAAI Conference on Artificial Intelligence*, **34**, 1234–1241 (2020).
22. Guo, S., Lin, Y., Feng, N., Song, C. & Wan, H. Attention based spatial-temporal graph convolutional networks for traffic flow forecasting. In *Proceedings of the AAAI Conference on Artificial Intelligence*, **33**, 922–929 (2019).

23. Alet, F., Weng, E., Lozano-Pérez, T. & Kaelbling, L. P. Neural relational inference with fast modular meta-learning. *Adv. Neural Inf. Process. Syst.* **32**, 11827–11838 (2019).
24. Zhang, Z. et al. A general deep learning framework for network reconstruction and dynamics learning. *Appl. Netw. Sci.* **4**, 1–17 (2019).
25. Pareja, A. et al. Evolvegn: Evolving graph convolutional networks for dynamic graphs. In *Proceedings of the AAAI Conference on Artificial Intelligence*, **34**, 5363–5370 (2020).
26. Franceschi, L., Niepert, M., Pontil, M. & He, X. Learning discrete structures for graph neural networks. In *International conference on machine learning*, 1972–1982 (PMLR, 2019).
27. Pearl, J. *Causality* (Cambridge university press, 2009).
28. Tank, A., Covert, I., Foti, N., Shojaie, A. & Fox, E. Neural granger causality for nonlinear time series. Preprint at <https://arxiv.org/abs/1802.05842> (2018).
29. Löwe, S., Madras, D., Zemel, R. & Welling, M. Amortized causal discovery: Learning to infer causal graphs from time-series data. Preprint at <https://arxiv.org/abs/2006.10833> (2020).
30. Glymour, C., Zhang, K. & Spirtes, P. Review of causal discovery methods based on graphical models. *Front. genetics* **10**, 524 (2019).
31. Peng, J., Wang, P., Zhou, N. & Zhu, J. Partial correlation estimation by joint sparse regression models. *J. Am. Stat. Assoc.* **104**, 735–746 (2009).
32. Stuart, J. M., Segal, E., Koller, D. & Kim, S. K. A gene-coexpression network for global discovery of conserved genetic modules. *Science* **302**, 249–255 (2003).
33. Stetter, O., Battaglia, D., Soriano, J. & Geisel, T. Model-free reconstruction of excitatory neuronal connectivity from calcium imaging signals. *PLoS Comput. Biol* **8**, e1002653 (2012).
34. Nitzan, M., Casadiego, J. & Timme, M. Revealing physical interaction networks from statistics of collective dynamics. *Sci. advances* **3**, e1600396 (2017).
35. Timme, M. & Casadiego, J. Revealing networks from dynamics: an introduction. *J. Phys. A: Math. Theor.* **47**, 343001(2014).
36. Liu, H., Kim, J. & Shlizerman, E. Functional connectomics from neural dynamics: probabilistic graphical models for neuronal network of *Caenorhabditis elegans*. *Philos. Transactions Royal Soc. B: Biol. Sci.* **373**, 20170377 (2018).
37. Runge, J. Causal network reconstruction from time series: From theoretical assumptions to practical estimation. *Chaos: An Interdiscip. J. Nonlinear Sci.* **28**, 075310 (2018).
38. Casadiego, J., Nitzan, M., Hallerberg, S. & Timme, M. Model-free inference of direct network interactions from nonlinear collective dynamics. *Nat. communications* **8**, 1–10 (2017).
39. Li, L., Xu, D., Peng, H., Kurths, J. & Yang, Y. Reconstruction of complex network based on the noise via QR decomposition and compressed sensing. *Sci. reports* **7**, 1–13 (2017).
40. Granger, C. W. Investigating causal relations by econometric models and cross-spectral methods. *Econom. journal Econom. Soc.* 424–438 (1969).
41. Sugihara, G. et al. Detecting causality in complex ecosystems. *Science* **338**, 496–500 (2012).
42. Ma, C., Chen, H.-S., Lai, Y.-C. & Zhang, H.-F. Statistical inference approach to structural reconstruction of complex networks from binary time series. *Phys. Rev. E* **97**, 022301 (2018).
43. Pathak, J., Hunt, B., Girvan, M., Lu, Z. & Ott, E. Model-free prediction of large spatiotemporally chaotic systems from data: A reservoir computing approach. *Phys. review letters* **120**, 024102 (2018).
44. Velickovic, P. et al. Graph attention networks. In *International Conference on Learning Representations* (OpenReview.net, 2018)

45. Wang, D. et al. Learning attribute-structure co-evolutions in dynamic graphs. Preprint at <https://arxiv.org/abs/2007.13004> (2020).
46. Velickovic, P. et al. Pointer graph networks. *Stat* **1050**, 11 (2020).
47. Wu, Z., Pan, S., Long, G., Jiang, J. & Zhang, C. Graph wavenet for deep spatial-temporal graph modeling. In *Proceedings of the Twenty-Eighth International Joint Conference on Artificial Intelligence, IJCAI-19*, 1907–1913 (IJCAI, 2019).
48. Li, Y., Meng, C., Shahabi, C. & Liu, Y. Structure-informed graph auto-encoder for relational inference and simulation. In *ICML Workshop on Learning and Reasoning with Graph-Structured Data* **8**, (2019).
49. Ayed, I., de Bézenac, E., Pajot, A., Brajard, J. & Gallinari, P. Learning dynamical systems from partial observations. Preprint at <https://arxiv.org/abs/1902.11136> (2019).
50. Pearl, J. & Mackenzie, D. *The Book of Why: The New Science of Cause and Effect* (Basic Books, 2018).
51. Baggio, G., Bassett, D. S. & Pasqualetti, F. Data-driven control of complex networks. Preprint at <https://arxiv.org/abs/2003.12189> (2020).
52. Baydin, A. G., Barak, P., Radul, A. A. & Siskind, J. Automatic differentiation in machine learning: a survey. *J. Mach. Learn. Res.* **18**, 1–43 (2018).
53. Gardiner, C. W. et al. *Handbook of Stochastic Methods* **3** (springer Berlin, 1985).
54. Hochreiter, S. & Schmidhuber, J. Long short-term memory. *Neural computation* **9**, 1735–1780 (1997).
55. Schölkopf, B. Causality for machine learning. Preprint at <https://arxiv.org/abs/1911.10500> (2019).
56. Jang, E., Gu, S. & Poole, B. Categorical reparameterization with gumbel-softmax. In *Fifth International Conference on Learning Representations, ICLR* (OpenReview.net, 2017).
57. Doersch, C. Tutorial on variational autoencoders. Preprint at <https://arxiv.org/abs/1606.05908> (2016).
58. Lee, J. et al. Deep neural networks as gaussian processes. In *Sixth International Conference on Learning Representations, ICLR* (OpenReview.net, 2018).
59. Brockmann, D. & Helbing, D. The hidden geometry of complex, network-driven contagion phenomena. *Science* **342**, 1337–1342 (2013).
60. Karlebach, G. & Shamir, R. Modelling and analysis of gene regulatory networks. *Nat. Rev. Mol. Cell Biol.* **9**, 770–780(2008).
61. Barzel, B. & Barabási, A.-L. Network link prediction by global silencing of indirect correlations. *Nat. biotechnology* **31**, 720–725 (2013).
62. Garcia, P., Parravano, A., Cosenza, M., Jiménez, J. & Marcano, A. Coupled map networks as communication schemes. *Phys. Rev. E* **65**, 045201 (2002).
63. Jalan, S., Amritkar, R. & Hu, C.-K. Synchronized clusters in coupled map networks. i. numerical studies. *Phys. Rev. E* **72**, 016211 (2005).
64. Campbell, A., Gurin, G. & Miller, W. E. *The Voter Decides*. (Row, Peterson, and Co., 1954).
65. Erdos, P. & Rényi, A. On the evolution of random graphs. *Publ. Math. Inst. Hung. Acad. Sci* **5**, 17–60 (1960).
66. Barabási, A.-L. & Albert, R. Emergence of scaling in random networks. *Science* **286**, 509–512 (1999).
67. Schaffter, T., Marbach, D. & Floreano, D. Genenetweaver: in silico benchmark generation and performance profiling of network inference methods. *Bioinformatics* **27**, 2263–2270 (2011).
68. Rossi, R. & Ahmed, N. The network data repository with interactive graph analytics and visualization. In *Proceedings of the AAAI Conference on Artificial Intelligence* **29**, 4292–4293 (AAAI Press, 2015)
69. Mengyuan Chen. et al. Inference for network structure and dynamics from time series data via graph neural network. Preprint at <https://arxiv.org/abs/2001.06576> (2020).
70. Tang, C. & Salakhutdinov, R. R. Multiple futures prediction. In *Advances in Neural Information Processing Systems*, 15398–15408 (2019).

## **Acknowledgements (not compulsory)**

We acknowledge Prof. Qinghua Chen, Dr. Lifei Wang, and the workshops in Swarna Club for the helpful discussion. We acknowledge the support of the National Natural Science Foundation of China (NSFC) under grant numbers 61673070.

## **Author contributions statement**

J.Z. conceived the experiments, Y.Z. and Y.G. conducted most of the experiments. Z.Z. and S.W. conducted the experiments on gene networks, M.Y.C. conducted the experiments of robustness. J.Z., Y.Z., and Y.G. wrote, and all authors reviewed the manuscript.

## **Competing interests**

The authors declare no competing interests.